On the numerical modeling of carbonation phenomenon via multi-reactional kinetics and 3D-randomly distributed spherical grains

Jena JEONG[*,a], Hamidréza. RAMÉZANI[b], Edgar CHUTA[a]

a. Université Paris-Est, Institut de Recherche en Constructibilité, ESTP, 28 Avenue Président Wilson, 94234 Cachan, France, jjeong@estp-paris.eu, jena.jeong@gmail.com, echuta@estp-paris.eu

b. École Polytechnique de l'Université d'Orléans, Université d'Orléans, ICMN, UMR CNRS 7374, Interfaces, Confinement, Matériaux et Nanostructures, 8 rue Léonrad de Vinci, 45072 Orléans, France, hamidreza.ramezani@univ-orleans.fr, hamidreza.ramezzani@gmail.com

Résumé :

A travers cet article, la modélisation mathématique et la solution numérique du phénomène de la carbonatation ont été étudiées pour les mortiers poreux. Pour cet objectif, la modélisation analytique proposée par Papadakis a été appliquée afin d'estimer les variations de concentration molaire de l'hydrate (CSH et $Ca(OH)_2$) et également les produits non déshydratés (C_2S et C_3S) pendant la carbonatation. Les simulations numériques ont d'abord été réalisées sur les échantillons numériques de mortier 3D, en considerant la présence des agrégats via la granulométrie respective pour que les applications présentent des résultats plus réalistes. La solution a été obtenue en utilisant la méthode des éléments finis pour un systéme transitoire non linéaire. Les résultats numériques ont été comparés à ceux réaliés à partir des essais expérimentales des carbonatations de faible et de forte concentration de CO_2. La zone carbonatée a été determinée par le détecteur de pH et l'analyse thermique différentielle (DTA). Certaines conclusions et perspectives relatives à la modélisation de la carbonatation ont été soulignées

Abstract :

In the present contribution, the mathematical modeling and numerical solution of the carbonation phenomenon have been investigated for the porous cement mortars. To achieve this goal, the Papadakis analytical proposal has been fully investigated. The molar concentration variations of the hydrate (CSH et $Ca(OH)_2$) and unhydrated products (C_2S et C_3S) have been analyzed during the carbonation. The numerical simulations have been firstly achieved on the 3D numerical mortar samples including the aggregates using the relevant granulometry, whose applications sustain more realistic outcomes. The solution has been done using the FEM for the non-linear transient system of PDEs. The numerical results have been compared to those done from the experiments using the pH detector and Differential Thermal Analysis (DTA). Some conclusions and outlooks pertaining to the carbonation modeling have been emphasized.

Mots clefs : low and high accelerated carbonation, numerical modeling, cement hydration, multi-reactional modeling, 3D-FEM

1 Introduction

In fact, Ordinary Portland Cement (OPC)-based materials are exposed to CO_2 gas in air or water including CO_2 gas, the carbonic acid neutralizes the alkalies in the pore water. So, some dominant hydration products like the calcium silicate hydrate gel ($C-S-H$) and calcium hydroxide ($Ca(OH)_2$) are dissolved by the acidic environment. As acid attack proceeds, dissolution of primary cementitious phases and the precipitation of second phases $CaCO_3$ result. In that acid environment, the reinforcement concrete cause the corrosion problem in structure concrete. In Table 1, some empirical and or semi-empirical carbonation depth estimations have been summarized as following

TABLE 1 – Brief literature survey of the empirical and/or semi-empirical carbonation depth estimations.

Papadakis *et al.* [1, 2]	$x_c = \left(\sqrt{\frac{2\mathrm{D}^{\mathrm{Pap}}[\mathrm{CO_2}]_0}{[\mathrm{CH}]_0 + 3[\mathrm{CSH}]_0 + 3[\mathrm{C_3S}]_0 + 2[\mathrm{C_2S}]_0}}\right)\sqrt{t}$
DuraCrete [3]	$x_c = \left(\left(\sqrt{\frac{2\mathrm{k_e k_c D}^{\mathrm{Dura}}\Delta C}{\mathrm{a}_{\mathrm{Dura}}}}\right)\left(\frac{t_0}{t}\right)^{w_{\mathrm{Dura}}}\right)\sqrt{t}$
Houst et Wittmann [4]	$x_c = \left(\sqrt{\frac{2\mathrm{cD}^{\mathrm{Hou}}}{\mathrm{a}_{\mathrm{Hou}}}}\right)\sqrt{t}$
Hyvert *et al.* [5]	$x_c = \left(\sqrt{\frac{2\mathrm{k_e k_c k_T D}^{\mathrm{Hyv}}\mathrm{P}_{\mathrm{CO_2}}}{\varphi_H RT\left(C_1 + \frac{C_2}{n_H+1}\left(\frac{\mathrm{P}_{\mathrm{CO_2}}}{\mathrm{P}_{\mathrm{atm}}}\right)^{n_H}\right)\left(1+\alpha_H C_2\left(\frac{\mathrm{P}_{\mathrm{CO_2}}}{\mathrm{P}_{\mathrm{atm}}}\right)^{n_H}\right)}}\right)\sqrt{t}$

in Table 1, $[CO_2]_0$, $[CH]_0$, $[CSH]_0$, $[C_3S]_0$, $[C_2S]_0$, and D^{Pap} are the initial CO_2 gas concentration, initial concentration of CH, initial concentration of CSH, initial concentration of C_3S, initial concentration of C_2S and effective diffusion coefficient of CO_2 through the carbonated concrete, respectively. For the DuraCrete relation proposal [3] in Table 1, k_e, k_c, ΔC, a_{Dura}, t_0, w_{Dura} and D^{Dura} are the environmental coefficient of DuraCrete model, curing coefficient of DuraCrete model, subtraction of the CO_2 concentration at the carbonation depth and uncarbonated zone beyond the carbonation depth region, concentration of carbonatable products, reference time, time scaling exponent coefficient and effective diffusion coefficient of CO_2 through the carbonated concrete at reference time (t_0), respectively. The Houst-Wittmann's model [4] contains c as subtraction of the CO_2 concentration at the carbonation depth and uncarbonated zone beyond the carbonation depth region, D^{Hou} as the diffusion coefficient of CO_2 and lastly, a_{Hou} as the concentration of carbonatable products. In the last model, i.e. Hyvert *et al.* model [5] represented in Table 1, k_e, k_c, k_T, P_{CO_2}, P_{atm}, C_1, C_2, φ_H, n_H, α_H and D^{Hyv} are the environmental coefficient, curing coefficient, thermal effects coefficient, CO_2 pressure at the external surfaces of concrete samples, atmospheric pressure or so-called ambient pressure, first initial concentration of calcium in the cement paste, second initial concentration of calcium, volumetric fraction of cement paste, Hyvert's exponent coefficient, Hyvert's C_2 multiplier coefficient and diffusion coefficient of carbonation affected zone in function of porosity, respectively. Some other relevant studies in conjunction with the cement and concrete carbonation can be also addressed in [6–11]. In all of analytical approaches based on ion mass transfer model and kinetic of ion exchange, Papadakis's proposal becomes more interesting due to the fact that the hydration phenomenon is taken into account using that not only calcium-silicate-hydroxide (C-S-H) and calcium hydroxide hydration $(CaOH)_2$ are going on during the carbonation but also anhy-

drous grains, C_2S and C_3S can continue its hydration with available pore water as well as with CO_2 gas. It is important to note that C1 and C2 of Hyvert's model also considers different calcium based forms. Even if Papadakis proposed a final very simplest solution of carbonation depth determination in the table, the authors will investigate in his original multi-reaction ion-exchange-transfer mass equilibrium model based on the system of time dependent differential equation. The numerical solution resolution is done via COMSOL-MATLAB code and then compared with ones from experiments according to low (10%) and high (75 %) accelerated carbonation during at very early step. Our contribution is highlighted as following ;

1. Low (10 %) and high (75 %) carbonation are performed on Portland (type CEMI) based cementitous materials, mortar specimens.
2. Partial and full carbonations are determined via numerical resolutions and experiments verification.
3. Front carbonation progress modeling is done taking into account the hydration of hydrate products and anhydrous gains too using Papadakis' proposal.
4. Two pH detectors, Phenolphthalein and Thymophtaleine are used to capture the pH change during the carbonation and their values are compared with DTG data.

2 Ion exchange equilibrium approach based on the Papadakis' method

2.1 Assumptions in cement carbonation modeling

In this sub-section, the mathematical modeling of the carbonation phenomenon is reviewed and generalized based on the Papadakis' landmark work [1, 2, 12, 13]. In the original Papadakis' study, one-dimensional modeling interpreting the physiochemical process was suggested using the relevant assumptions as following :

— The chemical reactions from which carbonatable materials are produced
— The diffusion of atmospheric CO_2 in the gaseous phase of the concrete pore
— The dissolution of solid $Ca(OH)_2$ in the pore water and the diffusion of dissolved $Ca(OH)_2$ in the aqueous phase of the pores
— The dissolution of CO_2 in the pore water and its reaction with dissolved $Ca(OH)_2$
— The reaction of CO_2 with the other solid carbonatable constituent of hardened cement paste
— The reduction of pore volume due to the solid products of hydration and carbonation
— The condensation of water vapor on the walls of concrete pores, in equilibrium to the ambient temperature and relative humidity condition

2.2 Ion exchange kinetic equilibrium based modeling

Based on the mass balance equations of the multi-reactional carbonation phenomenon, mathematical modeling is presented as the system of partial differential equations as following :

$$\int_{\Omega^{\mathrm{CP}}(t)} \frac{\partial \left(\mathrm{P}\left(1-\mathrm{f}\right)\left[\mathrm{CO_2}\right]\right)}{\partial t}\, dV = \int_{\Omega^{\mathrm{CP}}(t)} \left(\overbrace{-\mathrm{Div}\left(-D_{\mathrm{e},\mathrm{CO_2}} \nabla\left(\left[\mathrm{CO_2}\right]\right)\right)}^{\text{Diffusive term}} \overbrace{-\mathrm{P}_0\, \mathrm{f_w} \mathrm{r_{CH}} - 3\,\mathrm{r_{CSH}} - 3\,\mathrm{r_{C_3S}} - 2\mathrm{r_{C_2S}}}^{\text{Sink terms due to CH, CSH, } C_3S \text{ and } C_2S} \right) dV \tag{1a}$$

$$\int_{\Omega^{\mathrm{CP}}(t)} \frac{\partial[\mathrm{Ca(OH)_2(s)}]}{\partial t}\, dV = \int_{\Omega^{\mathrm{CP}}(t)} \left(\overbrace{r_{\mathrm{H,CH}}}^{\text{Source term due to CH}} \quad \overbrace{-\mathrm{P_0\, f_w\, r_{CH}}}^{\text{Sink term due to Ca(OH)}_2\text{(s) dissolution rate}} \right) dV \tag{1b}$$

$$\int_{\Omega^{\mathrm{CP}}(t)} \frac{\partial[\mathrm{CSH}]}{\partial t}\, dV = \int_{\Omega^{\mathrm{CP}}(t)} \left(\overbrace{-\mathrm{r_{CSH}}}^{\text{Sink term due to CSH}} \quad \overbrace{+\mathrm{r_{H,CSH}}}^{\text{Source term due to CSH}} \right) dV \tag{1c}$$

$$\int_{\Omega^{\mathrm{CP}}(t)} \frac{\partial[\mathrm{C_3S}]}{\partial t}\, dV = \int_{\Omega^{\mathrm{CP}}(t)} \left(\overbrace{-\mathrm{r_{C_3S}}}^{\text{Sink term due to C}_3\text{S}} \quad \overbrace{-\mathrm{r_{H,C_3S}}}^{\text{Sink term due to C}_3\text{S during the hydration}} \right) dV \tag{1d}$$

$$\int_{\Omega^{\mathrm{CP}}(t)} \frac{\partial[\mathrm{C_2S}]}{\partial t}\, dV = \int_{\Omega^{\mathrm{CP}}(t)} \left(\overbrace{-\mathrm{r_{C_2S}}}^{\text{Sink term due to C}_2\text{S}} \quad \overbrace{+\mathrm{r_{H,C_2S}}}^{\text{Sink term due to C}_2\text{S during hydration}} \right) dV \tag{1e}$$

where, Ω^{CP} represents the cement paste medium only due to the fact that sand aggregates does not react with CO2 gas. The reaction rate of each constituent with CO_2 is showed like

$$\mathrm{r}_j = k_j\, a_s\, [j]\, \bar{V}_j\, [\mathrm{CO_2}] \quad \text{for} \quad j = \mathrm{CSH, C_3S, C_2S} \tag{2}$$

where $[j]$, k_j, a_s, $\bar{V}_j$ and [CO_2] stand for the molar concentration of constituent j (in moles per unit volume of concrete), rate constant for the reaction of constituent j with CO_2, specific surface area of concrete pores in contact with water, the molar volume of constituent j and CO_2 molar concentration, respectively. Alors, the reaction rate of CO_2 with dissolved $Ca(OH)_2$, $\mathrm{r_{CH}}$ is proposed as below :

$$\mathrm{r_{CH}} = H\, R\, T\, k_2\, [\mathrm{OH^-_{eq}}] \tag{3}$$

where, [CO_2], H, R, T and k_2 are the CO_2 molar concentration in gaseous phase, Henry's constant for the dissolution of CO_2 in water H = 34.2 [$\frac{mol}{m^3 atm}$] (at 25°C), gas constant $R = 8.206 \times 10^{-5}$ [$\frac{m^3 atm}{mol.K}$], absolute temperature in Kelvin and rate constant for CO_2 and OH^-, which is equal to 8.3 [$\frac{m^3}{mol.sec}$], respectively. In the diffusion term in Eq. 1a, $D_{e,\mathrm{CO_2}}$ signifies an effective diffusivity from regions where the CO_2 concentration is high to those where is it low. One of the very interesting aspect is that the porosity P is taken into account for the computations in according to the mathematical framework. In fact, $\mathrm{P_0}$ represents the initial porosity and $\mathrm{P}(t)$ is the current porosity whose value can be extracted via the constantly growing hydration and carbonation reactions as follows :

$$\mathrm{P}(t) = \mathrm{P_0} - \Delta\mathrm{P_H}(t) - \Delta\mathrm{P_C}(t) \tag{4}$$

where, $\mathrm{P}(t)$, $\mathrm{P_0}$, $\Delta\mathrm{P_H}(t)$ and $\Delta\mathrm{P_C}(t)$ are the current porosity, the initial porosity, the porosity reduction stemming from the hydration and the porosity reduction coming from the carbonation, respectively. In the next section, we focus on the numerical experiments of 3D mortar samples in accordance with the extension of Papadakis' landmark mathematical modeling.

3 Numerical experiments

In this section, the numerical modeling of the carbonation of numerical mortar cube of 20 mm including sand grains in Figure 1 has been done. The use of randomly distributed spherical grains through the cement paste can include the effect of corners, curvature, even surface roughness whose existence would affect the CO2 diffusion across porous cement paste materials in an implicit manner. Furthermore, the multi-reactional modeling including the grains is an essential tool to assess the pH distribution across the cement paste and provide some essential ideas about the carbonation testing techniques in evaluating the pH values. To obtain the accurate numerical outcomes, fairly fine mesh density has been applied for the numerical experiments. The quadratic isoparametric Lagrange elements are used for the meshing purposes herein. By applying the symmetry assumptions as described before, the following boundary

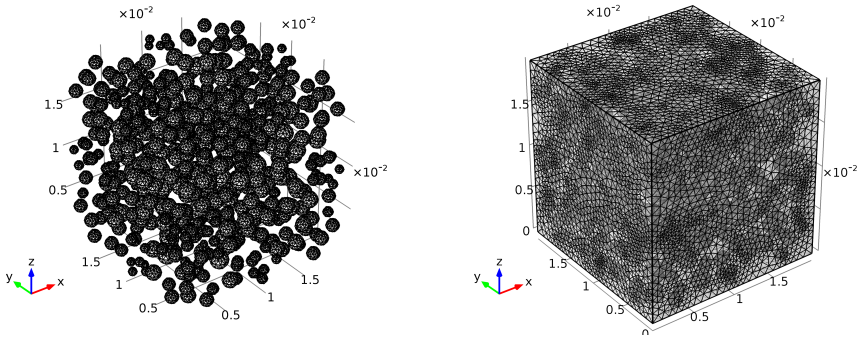

(a) (b)

FIGURE 1 – Mesh density illustration including the aggregates and cement paste matrix, a) Aggregates mesh density and b) Aggregates and cement paste matrix mesh densities.

conditions would be kept during the computations :

The boundary conditions over the symmetry planes, i.e. XY, YZ and ZX yield no-flux flow conditions. This implies the following Neumann's boundary conditions as :

Symmetry boundary conditions for [CO_2] :

$$\begin{cases} -D_{\mathrm{e,CO_2}}\dfrac{\partial[\mathrm{CO_2}]}{\partial x}=0 \quad \text{on} \quad \partial\Omega^{\mathrm{yz}}\subset\mathbb{R}^2 \qquad \partial\Omega^{\mathrm{yz}}=\{S\in\mathbb{R}^2|\, x=0, 0\leqslant y\leqslant 20, 0\leqslant z\leqslant 20\} \\ -D_{\mathrm{e,CO_2}}\dfrac{\partial[\mathrm{CO_2}]}{\partial y}=0 \quad \text{on} \quad \partial\Omega^{\mathrm{xz}}\subset\mathbb{R}^2 \qquad \partial\Omega^{\mathrm{xz}}=\{S\in\mathbb{R}^2|\, y=0, 0\leqslant x\leqslant 20, 0\leqslant z\leqslant 20\} \\ -D_{\mathrm{e,CO_2}}\dfrac{\partial[\mathrm{CO_2}]}{\partial z}=0 \quad \text{on} \quad \partial\Omega^{\mathrm{xy}}\subset\mathbb{R}^2 \qquad \partial\Omega^{\mathrm{xy}}=\{S\in\mathbb{R}^2|\, z=0, 0\leqslant x\leqslant 20, 0\leqslant y\leqslant 20\} \end{cases} \tag{5}$$

Symmetry boundary conditions for [j]=[$Ca(OH)_2$(s)], [CSH], [C_3S] and [C_2S] :

$$\begin{cases} -\dfrac{\partial[\mathrm{j}]}{\partial x}=0 \quad \text{on} \quad \partial\Omega^{\mathrm{yz}}\subset\mathbb{R}^2 \quad \partial\Omega^{\mathrm{yz}}=\{S\in\mathbb{R}^2|\, x=0, 0\leqslant y\leqslant 20, 0\leqslant z\leqslant 20\} \\ -\dfrac{\partial[\mathrm{j}]}{\partial y}=0 \quad \text{on} \quad \partial\Omega^{\mathrm{xz}}\subset\mathbb{R}^2 \quad \partial\Omega^{\mathrm{xz}}=\{S\in\mathbb{R}^2|\, y=0, 0\leqslant x\leqslant 20, 0\leqslant z\leqslant 20\} \\ -\dfrac{\partial[\mathrm{j}]}{\partial z}=0 \quad \text{on} \quad \partial\Omega^{\mathrm{xy}}\subset\mathbb{R}^2 \quad \partial\Omega^{\mathrm{xy}}=\{S\in\mathbb{R}^2|\, z=0, 0\leqslant x\leqslant 20, 0\leqslant y\leqslant 20\} \end{cases} \tag{6}$$

The boundary conditions over the outer surfaces can be written as below :

Outer surfaces boundary conditions for [CO_2] :

$$\left\{[\mathrm{CO_2}] = [\mathrm{CO_2}]_0 \quad \text{on} \quad \partial\Omega^{\text{outer}} \subset \mathbb{R}^2 \quad \partial\Omega^{\text{outer}} = \{S \in \mathbb{R}^2 |\, x = 20\} \cup \{S \in \mathbb{R}^2 |\, y = 20\} \cup \{S \in \mathbb{R}^2 |\, z = 20\}\right. \tag{7}$$

where, $[\mathrm{CO_2}]_0$ signifies the initial molar concentration of carbon dioxide at the outer surfaces of the mortar samples.

The initial conditions can be denoted as below :

$$\begin{cases} [\mathrm{CO_2}](\mathbf{x}, 0) = 0 & \text{on} \quad \partial\Omega^{\text{CP}} \subset \mathbb{R}^3 \\ [\mathrm{Ca(OH)_2(s)}](\mathbf{x}, 0) = [\mathrm{Ca(OH)_2(s)}]_0 & \text{on} \quad \partial\Omega^{\text{CP}} \subset \mathbb{R}^3 \\ [\mathrm{CSH}](\mathbf{x}, 0) = [\mathrm{CSH}]_0 & \text{on} \quad \partial\Omega^{\text{CP}} \subset \mathbb{R}^3 \\ [\mathrm{C_3S}](\mathbf{x}, 0) = [\mathrm{C_3S}]_0 & \text{on} \quad \partial\Omega^{\text{CP}} \subset \mathbb{R}^3 \\ [\mathrm{C_2S}](\mathbf{x}, 0) = [\mathrm{C_2S}]_0 & \text{on} \quad \partial\Omega^{\text{CP}} \subset \mathbb{R}^3 \\ \mathrm{P}(\mathbf{x}, 0) = \mathrm{P}_0 & \text{on} \quad \partial\Omega^{\text{CP}} \subset \mathbb{R}^3 \end{cases} \tag{8}$$

where, $[\mathrm{Ca(OH)_2(s)}]_0$, $[\mathrm{CSH}]_0$, $[\mathrm{C_3S}]_0$, $[\mathrm{C_2S}]_0$ and P_0 are the initial molar concentration of [$Ca(OH)_2$(s)], [CSH], [C_3S], [C_2S] and initial porosity, respectively [1].

4 Model verification via experiments

In this section, the numerical outcomes of the carbonation phenomenon extracted by means of the multi-reactional modeling issues are compared to the experiments. The carbonation experiments have been achieved in so-called low, i.e. 10% and high carbonation 75% conditions herein. The pH detector and Differential Thermal Analysis (DTA) are utilized to estimate the carbonation depth as a tool for the modeling assessment purposes. As pointed out previously, the multi-reactional modeling for the carbonation like that originally proposed by Papadakis, gets the spatial distribution of CO_2, $Ca(OH)_2$, CSH, C_3S and C_2S within carbonation time after the hydration process. To mimic the real conditions like those achieved for the experiments, the above-indicated modeling accounts for the hydration phenomenon as well. As a matter of fact, the carbonation and hydration phenomena go altogether in the same mathematical modeling framework using the weak form considerations.

4.1 Materials and experiments

As pointed out earlier, the applied cement is an Ordinary Portland Cement (OPC) based standard mortar, i.e. P45, Water-to-Cement ratio=0.5, has been used to prepare the mortar bars ($160 \times 40 \times 40\,[mm^3]$). The mortar specimens have been made and stored at 20°C including the $95 \pm 5\%$ of relative humidity during 28 days. After the hydration period (28 days), all specimens have been kept in the incubator at 20°C and $65 \pm 5\%$ during nearly 3 months. This wet curing period is necessary in order to conduct the same saturation through the specimen and to fulfill the carbonation test conditions. The applied relative humidity of $\approx 65\%$ is chosen in such a way to maximize the carbonation rate.

4.2 Low accelerated carbonation case

In the low accelerated carbonation case, the CO_2 gas concentration of 10% is applied for the numerical modeling and the carbonation experiments. The numerical solution is done at 3, 7, 14 and 22 days after

1. The relevant coefficients can be found out in the nomenclature.

carbonation. The CO_2 gas diffusion at 14 days of carbonation is illustrated in Figure 2. The effect of tortuosity caused from presence of aggregates is well delineated in Figure 2 where the diffusion-lines are interrupted via the aggregates.

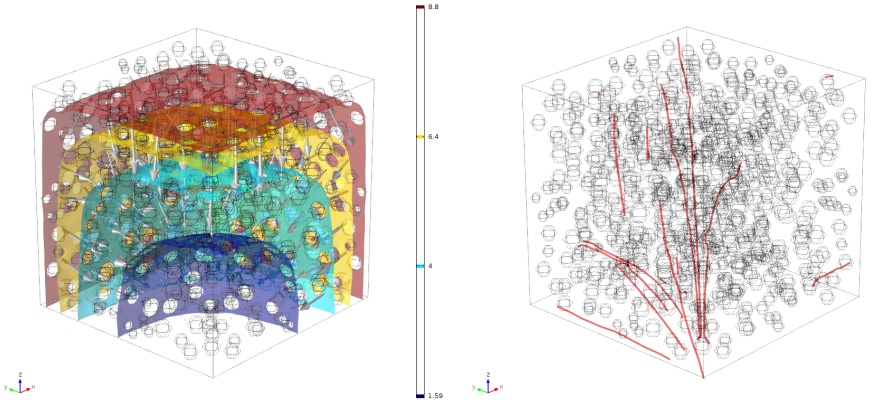

(a) (b)

FIGURE 2 – a) CO_2 distribution in 10% ([CO2]=10%) at 14 days after the carbonation action including CO_2 inward flux vector-field and b) CO_2 streamline diffusion in 10% ([CO2]=10%) at 14 days after the carbonation action.

The numerical results are shown in Figure 3 at 3, 7, 14 and 22 days of carbonation. As shown in Figure 3, the $Ca(OH)_2$ concentration is getting reduced drastically within the carbonation phenomenon after 14 days of carbonation while the very slow trend for the CSH, C_3S and C_2S can be found out. In fact, it is understood that two anhydrous products have been consumed via the carbonation reactions and hydration-based phenomena. The CSH is slowly increased within the carbonation. Moreover, this matter looks more colorful at the center of specimen than the outside surfaces. It might be the consumption of CSH during the hydration.

The Figure 4 shows the carbonated zone on all specimens at 3 and 14 days. For all pH detectors, the carbonated zone shows as uncolored zone while the color begins to appear when pH changes. According to the results, it could be observed that Thymophtaleine is more sensitive to the pH variations than Phenolphthalein as expected earlier. Indeed, the carbonated zone does not look very clear with the Phenolphthalein application due to the fact that the pink line does not look very clear. Moreover, one can observe some pink points even in the carbonated zone. It is necessary to emphasize that the carbonated zones are sliced and used for the DTA tests.

The Figure 5 illustrates DTA diagrams of carbonated zones at various carbonation days, i.e. 3, 7, 14 and 22 days as well as the uncarbonated zones. According to the DTA results, the partial carbonation can be observed i.e. the reduced CSH and ettringite quantity in the temperature range 110°C-130°C, $Ca(OH)_2$ for 460°C-510°C and calcite for 650°C-750°C. In fact, it is observed that the water evaporation is done and then it is not easy to be distinguished in an accurate manner among the water evaporation, CSH and/or ettringite. Furthermore, the carbonation may dry out the mortar as well.

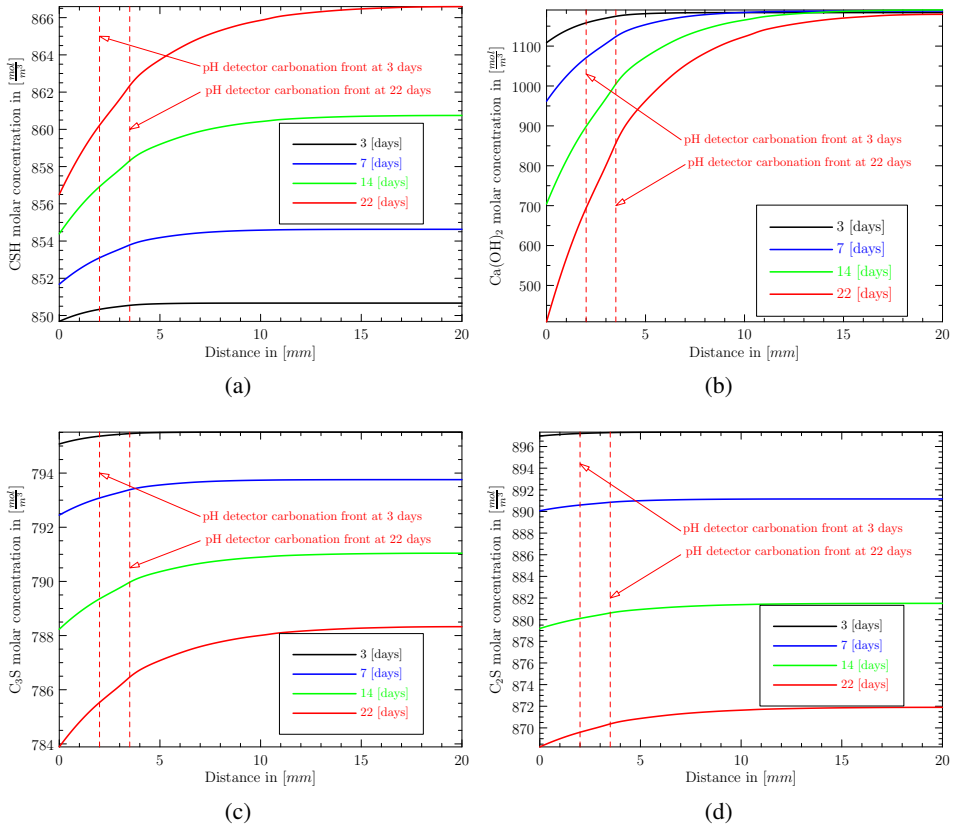

FIGURE 3 – Molar concentration versus distance at centerline on plane YZ with [CO_2]=10%, a) CSH concentration distribution in [$\frac{mol}{m^3}$] at 3, 7, 14 and 22 days after the carbonation action, b) $Ca(OH)_2$ concentration distribution in [$\frac{mol}{m^3}$] at 3, 7, 14 and 22 days after the carbonation action, c) C_3S concentration distribution in [$\frac{mol}{m^3}$] at 3, 7, 14 and 22 days after the carbonation action and d) C_2S concentration distribution in [$\frac{mol}{m^3}$] at 3, 7, 14 and 22 days after the carbonation action.

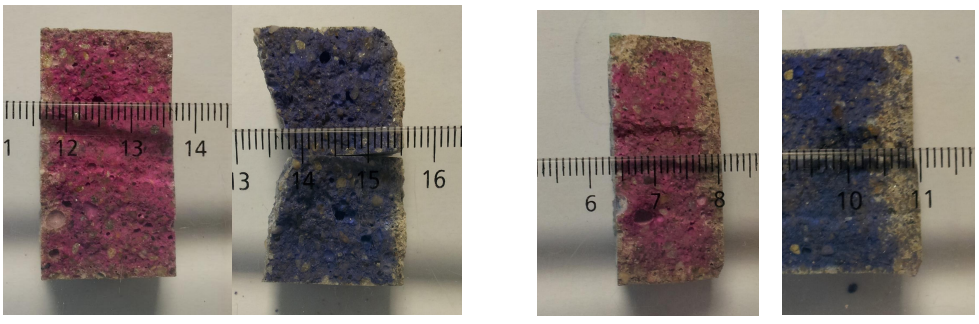

FIGURE 4 – Front carbonation capturing (10% carbonation) via pH detectors (the pink color for Phenolphthalein and blue color for Thymophtaleine).

4.3 High accelerated carbonation case

In high carbonation case, the 75% of CO_2 gas concentration is applied in the numerical modeling and the experiments. The CO_2 distribution at 14 days of carbonation is shown in Figure 6. In this figure, one can observe that the CO_2 diffusion is faster than the 10% case. The stream-line CO_2 diffusion clearly shows the diffusion can go directly toward center.

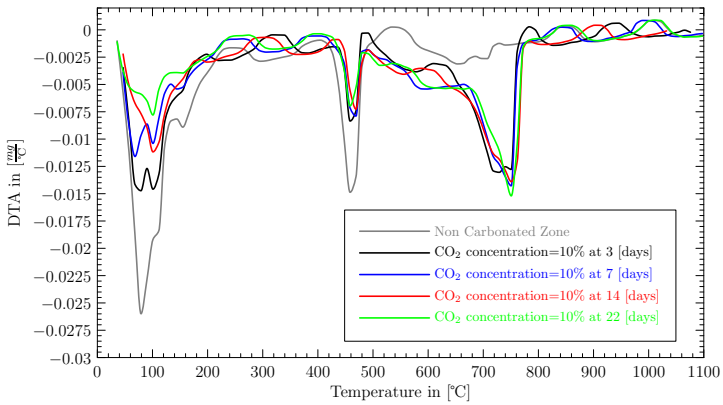

FIGURE 5 – DTA data of mortar samples extracted at the carbonated zone only after 3, 7, 14 and 22 days of carbonation action (low carbonation) comparing to the uncarbonated zone.

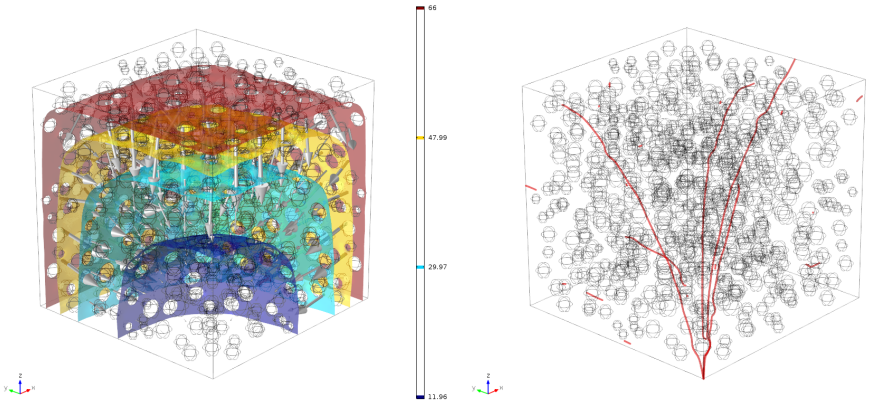

(a) (b)

FIGURE 6 – a) CO_2 distribution in 75% ([CO2]=75%) at 14 days after the carbonation action including CO_2 inward flux vector-field and b) CO_2 streamline diffusion in 10% ([CO2]=75%) at 14 days after the carbonation action.

The numerical results for high carbonation case are depicted in Figure 7. According to the outcomes, the $Ca(OH)_2$ is entirely consumed at 7 days after carbonation next to the external surfaces. However, CSH shows a quite different trend. In fact, CSH is reduced at the external surface but the CSH increases more and more around the center of the mortar. It may be due to the steadily hydration phenomenon progress with two anhydrous grains, i.e. C_2S and C_3S. It is observed that there are two issues. The first one is the creation of CSH within the hydration and the second one is the consumption of CSH due to the carbonation issues. For high carbonation, the CSH consumption is too much bigger than its creation during the carbonation.

The high concentration of CO_2 exhibits some interesting features. The carbonation front capturing via the pH detectors is displayed in Figure 8. Comparing to the low carbonation case, the carbonation front is not as clear as the low carbonation at the early age. Nevertheless, the carbonation seems to progress at 14 days very fast. Hence, the detected zone is larger than that of low carbonation.

Based on the DTA tests, for both low 10% Figure 5 and high 75% concentration Figure 9, $CaCO_3$ seems to be mainly decomposed at lower temperatures, 680°C-780°C. However, in high carbonation case, CSH quantity is greater than low carbonation case and thus it sharply declines. This matter means that the high CO_2 concentration sustains slow carbonation at the early age and then it speeds up very fast. It

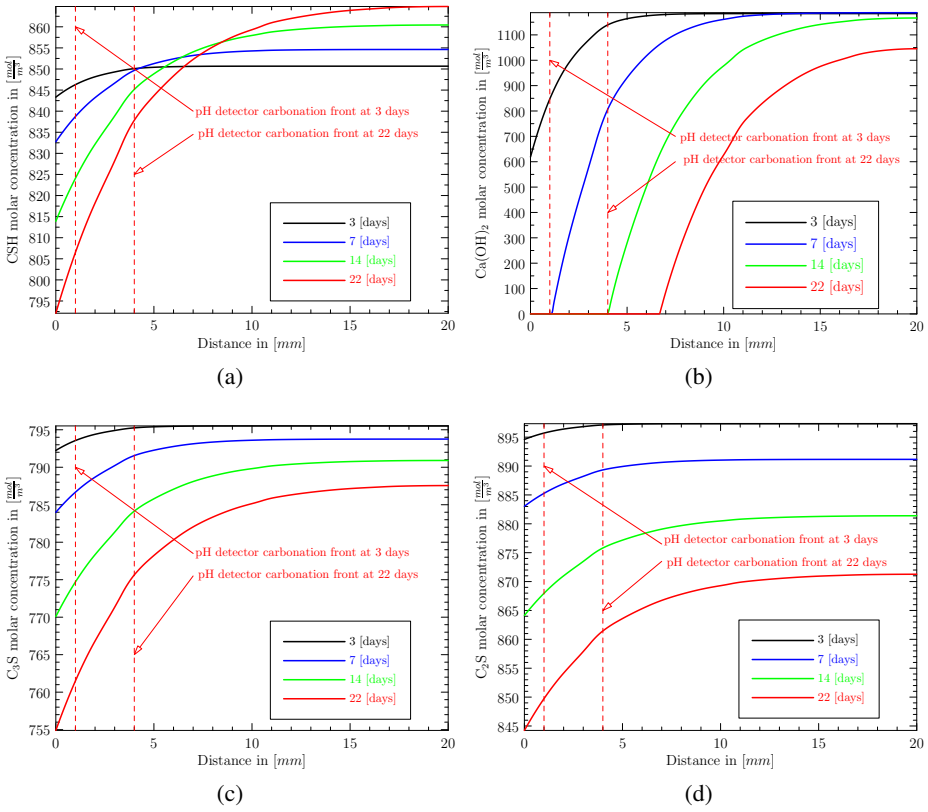

FIGURE 7 – Molar concentration versus distance at centerline on plane YZ with [CO_2]=75%, a) CSH concentration distribution in $[\frac{mol}{m^3}]$ at 3, 7, 14 and 22 days after the carbonation action, b) $Ca(OH)_2$ concentration distribution in $[\frac{mol}{m^3}]$ at 3, 7, 14 and 22 days after the carbonation action, c) C_3S concentration distribution in $[\frac{mol}{m^3}]$ at 3, 7, 14 and 22 days after the carbonation action and d) C_2S concentration distribution in $[\frac{mol}{m^3}]$ at 3, 7, 14 and 22 days after the carbonation action.

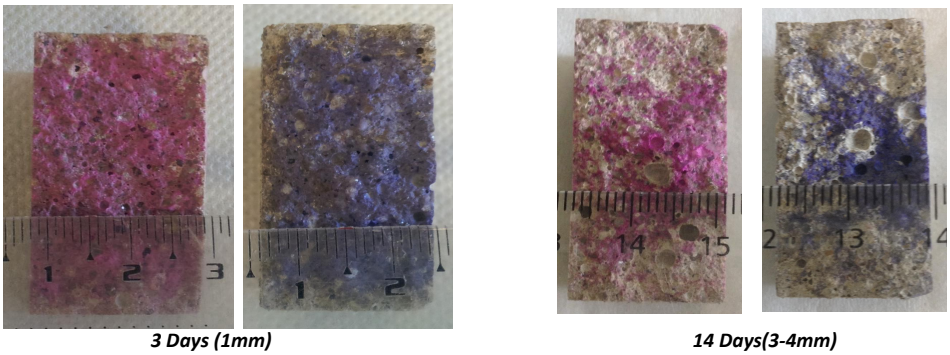

FIGURE 8 – Front carbonation capturing (75% carbonation) via pH detectors (the pink color for Phenolphthalein and blue color for Thymophtaleine).

is well worth noting that $Ca(OH)_2$ can be progressively dissolved and thus $Ca(CO)_3$ is produced much greater than low carbonation case.

According to the numerical solution, $Ca(OH)_2$ has been fully dissolved in 7 days after the carbonation. Nevertheless, the DTA findings demonstrate that $Ca(OH)_2$ is partially consumed. The latter observation

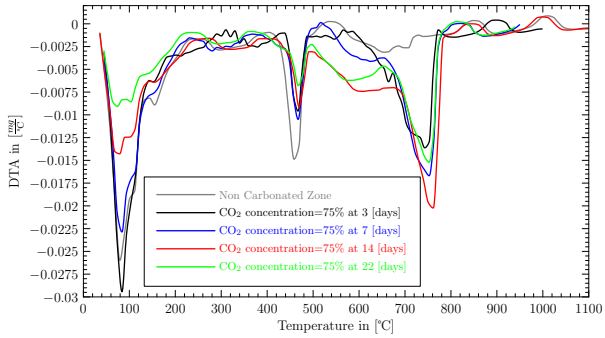

FIGURE 9 – DTA data of mortar samples extracted at the carbonated zone only after 3, 7, 14 and 22 days of carbonation action (high carbonation) comparing to the uncarbonated zone.

may be due to $Ca(CO)_3$ precipitation around $Ca(OH)_2$ which is not appropriately incorporated into the multi-reactional kinetics modeling herein.

5 Conclusions and outlooks

The comparison between the numerical modeling and experiments reveals some gaps. These gaps might come from the mathematical modeling issues. The latter modeling would idealize the carbonation phenomenon and then it does not take into account the complex precipitation of $Ca(CO)_3$ across cement mortar pore network at low carbonation case as well as high carbonation case. Basically, there are two issues which may alter the carbonation progress. The first one is the water production via the CO_2 chemical reactions. The second comes form the outcome of the water productions which is known as logging. The above-mentioned issues strongly depend on experiments setups and particularly, the CO_2 concentration values. As far as the authors' knowledge, a very few mathematical modeling can take it into consideration in an appropriate manner including the multi-reactional issues. Generally, the carbonation modelings can partly cover the carbonation issues for particular cases. It is straightforward to mention that this gets worse for the high carbonation conditions rather than low carbonation ones. Additionally, the above-indicated modeling would over-estimate the carbonation depth at low and high carbonation cases. Consequently, it can be concluded that the mathematical modeling based on the chemical reaction only would not be sufficient to predict the carbonation process. It should include the randomness features of pore networks and the relevant stochastic crystallization across the cement mortars as well as the water production leading to clogging issues. The next studies would focus on the inclusion of the full precipitation as well as random pore network issues using the chemo-mechanical aspects. One possible way to handle the last point is to use the micro-dilatation theory [14–23] as long as the ion-exchange issues.

Références

[1] V. G. Papadakis, C. G. Vayenas, and M. N. Fardis. A reaction engineering approach to the problem of concrete carbonation. *AIChE Journal*, 35(10) :1639–1650, 1989.

[2] V.G. Papadakis, C.G. Vayenas, and M.N. Fardis. Fundamental modeling and experimental investigation of concrete carbonation. *ACI Materials Journal*, 88(4) :363–373, July 1991. (Document Name : 88-M43).

[3] DuraCrete. General guidlines for durability design and redesign. Technical report, The European Union - BriteEuram III, 2000. (Project BE95-1347).

[4] Yves F. Houst and Folker H. Wittmann. Depth profiles of carbonates formed during natural carbonation. *Cement and Concrete Research*, 32(12) :1923–1930, 2002.

[5] N. Hyvert, A. Sellier, F. Duprat, P. Rougeau, and P. Francisco. Dependency of C–S–H carbonation rate on CO2 pressure to explain transition from accelerated tests to natural carbonation. *Cement and Concrete Research*, 40(11) :1582–1589, 2010.

[6] N. Al Akchar, V. Baroghel-Bouny, and A. Raharinaivo. Propagation du front de carbonatation dans les pâtes de ciment / carbonation front propagation in cement pastes. In *Science des matériaux et propriétés des bétons, Rencontres internationales*, volume 237 of *ATILH №37655*, pages 247–255, Toulouse, France, March 1998. (In French).

[7] B. Bary and A. Sellier. Coupled moisture-carbon dioxide-calcium transfer model for carbonation of concrete. *Cement and Concrete Research*, 34(10) :1859–1872, 2004.

[8] M. Thiery, G. Villain, P. Dangla, and G. Platret. Investigation of the carbonation front shape on cementitious materials : Effects of the chemical kinetics. *Cement and Concrete Research*, 37(7) :1047–1058, 2007.

[9] Leon Black, Krassimir Garbev, and Ian Gee. Surface carbonation of synthetic C-S-H samples : A comparison between fresh and aged C-S-H using X-ray photoelectron spectroscopy. *Cement and Concrete Research*, 38(6) :745–750, 2008.

[10] Qinghua Huang, Zhilu Jiang, Weiping Zhang, Xianglin Gu, and Xiaojing Dou. Numerical analysis of the effect of coarse aggregate distribution on concrete carbonation. *Construction and Building Materials*, 37 :27 – 35, 2012. (Non Destructive Techniques for Assessment of Concrete).

[11] Qian Zhang. Mathematical modeling and numerical study of carbonation in porous concrete materials. *Applied Mathematics and Computation*, 281 :16 – 27, 2016.

[12] Vagelis G. Papadakis, Costas G. Vayenas, and Michael N. Fardis. Experimental investigation and mathematical modeling of the concrete carbonation problem. *Chemical Engineering Science*, 46(5–6) :1333–1338, 1991.

[13] Vagelis G. Papadakis, Costas G. Vayenas, and Michael N. Fardis. Physical and chemical characteristics affecting the durability of concrete. *Materials Journal*, 88(2) :186–196, March 1991. (Document Name : 88-M24).

[14] Jace W. Nunziato and Stephen C. Cowin. A nonlinear theory of elastic materials with voids. *Archive for Rational Mechanics and Analysis*, 72(2) :175–201, June 1979.

[15] Stephen C. Cowin and Jace W. Nunziato. Linear elastic materials with voids. *Journal of Elasticity*, 13(2) :125–147, 1983.

[16] G. Iovane and A.V. Nasedkin. Finite element analysis of static problems for elastic media with voids. *Computers and Structures*, 84(1-2) :19–24, 2005.

[17] Hamidréza Ramézani, Holger Steeb, and Jena Jeong. Analytical and numerical studies on Penalized Micro-Dilatation (PMD) theory : Macro-micro link concept. *European Journal of Mechanics - A/Solids*, 34(0) :130–148, 2012.

[18] Jena Jeong, Paul Sardini, Hamidréza Ramézani, Marja Siitari-Kauppi, and Holger Steeb. Modeling of the induced chemo-mechanical stress through porous cement mortar subjected to CO2 :

Enhanced micro-dilatation theory and 14C-PMMA method. *Computational Materials Science*, 69(0) :466 – 480, 2013.

[19] Hamidréza Ramézani and Jena Jeong. Non-linear elastic micro-dilatation theory : Matrix exponential function paradigm. *International Journal of Solids and Structures*, 67-68(0) :1–26, 2015.

[20] Jena Jeong, Hamidréza Ramézani, Paul Sardini, Djimédo Kondo, Laurent Ponson, and Marja Siitari-Kauppi. Porous media modeling and micro-structurally motivated material moduli determination via the micro-dilatation theory. *The European Physical Journal Special Topics*, 224(9) :1805–1816, July 2015.

[21] J. Sladek, V. Sladek, M. Repka, and P.L. Bishay. Static and dynamic behavior of porous elastic materials based on micro-dilatation theory : A numerical study using the {MLPG} method. *International Journal of Solids and Structures*, 96 :126 – 135, 2016.

[22] Jena Jeong, Hamidréza Ramézani, and Peter Gosling. Multi-scale stochastic porous media modeling via the micro-dilatation theory : Concrete materials application. In *WCCM-APCOM 2016 Congress*, 24-29 July 2016.

[23] Jena Jeong, Hamidréza Ramézani, and Nordine Leklou. Porous-micro-dilatation theory for random crystallization : Monte carlo simulation for delayed ettringite formation. *Acta Mechanica*, pages 1–27, June 2017. (Available online).